

# MoSE: Unveiling Structural Patterns in Graphs via Mixture of Subgraph Experts

Junda Ye<sup>\*1,3</sup>, Zhongbao Zhang<sup>†1</sup>, Li Sun<sup>2</sup>, Siqiang Luo<sup>†3</sup>

<sup>1</sup>Beijing University of Posts and Telecommunications

<sup>2</sup>North China Electric Power University

<sup>3</sup>Nanyang Technological University

{jundaye, zhongbaobz}@bupt.edu.cn, ccesunli@ncepu.edu.cn, siqiang.luo@ntu.edu.sg

## Abstract

While graph neural networks (GNNs) have achieved great success in learning from graph-structured data, their reliance on local, pairwise message passing restricts their ability to capture complex, high-order subgraph patterns, leading to insufficient structural expressiveness. Recent efforts have attempted to enhance structural expressiveness by integrating random walk kernels into GNNs. However, these methods are inherently designed for graph-level tasks, which limits their applicability to other downstream tasks such as node classification. Moreover, their fixed kernel configurations hinder the model’s flexibility in capturing diverse subgraph structures. To address these limitations, this paper proposes a novel **Mixture of Subgraph Experts (MoSE)** framework for flexible and expressive subgraph-based representation learning across diverse graph tasks. Specifically, MoSE extracts informative subgraphs via anonymous walks and dynamically routes them to specialized experts based on structural semantics, enabling the model to capture diverse subgraph patterns with improved flexibility and interpretability. We further provide a theoretical analysis of MoSE’s expressivity within the Subgraph Weisfeiler-Lehman (SWL) Test, proving that it is more powerful than SWL. Extensive experiments, together with visualizations of learned subgraph experts, demonstrate that MoSE not only outperforms competitive baselines, but also provides interpretable insights into structural patterns learned by the model.

## Introduction

Graphs, serving as data structures capable of depicting complex relationships between entities, are ubiquitous in real-world scenarios, such as social networks (Yang et al. 2024; Liao et al. 2022; Liu, Liao, and Luo 2025), biological molecules (Hao et al. 2020; Rong et al. 2020), and recommendation systems (Wu et al. 2022; Yu et al. 2022). As a prominent approach for learning representations from graphs, graph neural networks (GNNs) have been widely studied (Defferrard, Bresson, and Vandergheynst 2016; Kipf and Welling 2017; Hamilton, Ying, and Leskovec 2017; Veličković et al. 2018; Xu et al. 2019) based on the philosophy of message-passing mechanism motivated by the Weisfeiler-Lehman (WL) graph isomorphism test (Leman

<sup>\*</sup>This work was completed while Junda Ye was a visiting PhD student at Nanyang Technological University.

<sup>†</sup>Co-Corresponding author.

and Weisfeiler 1968). These message passing neural networks (MPNNs) constitute the most prevailing type of GNNs, however, their expressive power is known to be upper bounded by the first-order Weisfeiler-Lehman (1-WL) isomorphism test (Xu et al. 2019). Moreover, recent research has demonstrated that such 1-WL equivalent GNNs lack sufficient expressive power to differentiate fundamental structural patterns such as triangles and cycles (Arvind et al. 2019; Chen et al. 2020).

As another line of work, graph kernel-based GNNs have attracted increasing attention in recent years due to their ability to bridge the provable theoretical guarantees of graph kernels with the expressive power of MPNNs (Mairal 2016; Lei et al. 2017; Al-Rfou, Perozzi, and Zelle 2019; Du et al. 2019; Chen, Jacob, and Mairal 2020; Cosmo et al. 2024). Among them, methods based on random walk kernel (RWK) have garnered particular interest due to their strong interpretability (Nikolentzos and Vazirgiannis 2020; Long et al. 2021; Lee, Zhao, and Akoglu 2024; Cosmo et al. 2024). These RWK-based GNNs typically compute similarities between the input graph and a set of learnable subgraphs, commonly referred to as hidden graphs, to derive graph-level representations. Each hidden graph serves as a structural probe and offers an interpretable way to capture recurring patterns across different datasets.

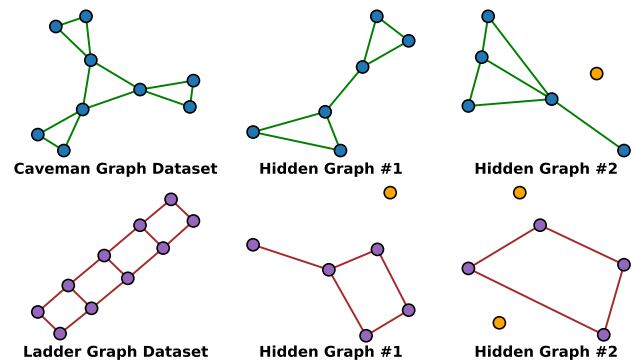


Figure 1: Hidden graphs learned by RWNN on Caveman and Ladder synthetic graph datasets. The hidden graph sizes are all fixed to 6. Redundant nodes, colored in orange, are **isolated** and contribute little to subgraph patterns.

Although RWK-based methods have achieved promising results, they still suffer from the following limitations. **First**, due to the computational complexity in calculating RWK, existing methods have primarily been constrained to graph-level tasks, which typically involve graphs with relatively fewer nodes. Consequently, these methods have seldom been applied to node-level tasks, thereby severely limiting their applicability to diverse real-world scenarios. While a few recent methods have attempted to extend RWK-based models to node-level tasks (Long et al. 2021; Lee, Zhao, and Akoglu 2024), they compute node representations by invoking RWK calculations or walk simulations over the entire graph, leading to high computational cost. **Second**, current models typically adopt pre-defined hidden graphs and fixed random walk lengths, and they treat each hidden graph equally, resulting in limited flexibility and adaptability. This rigid strategy limits the model’s capacity to adaptively represent optimal substructures, leading to redundancy and unnecessary computational overhead. We illustrate this with a case study in Fig. 1, where fixed hidden graph configurations lead to the inclusion of redundant nodes, ultimately incurring extra computational cost. These insights and limitations raise a natural question: *Can we design a more flexible and efficient RWK-based framework that adaptively supports feature and structure modeling for each node to better suit diverse graph tasks and scales while preserving interpretability?*

Toward this end, we propose MoSE, namely Mixture of Subgraph Experts, a new model grounded in the Mixture of Experts (MoE) paradigm, enabling each node to adaptively select subgraph experts from its local context. Specifically, we introduce a novel subgraph extraction strategy together with a subgraph-aware gating mechanism, which jointly helps subgraph experts to capture informative structural patterns. Compared to other RWK-based models, MoSE offers more refined interpretability, and an average 10.84% performance improvement at around 30% reduction in runtime. The interpretability is further supported by visualizations of the learned subgraph experts, which reveal compact and diverse structural patterns aligned with task semantics.

The major contributions of our work are summarized as follows:

- To the best of our knowledge, we are the first to introduce MoE into RWK-based graph neural networks, offering a flexible framework for modeling diverse subgraph patterns while retaining the semantic interpretability of kernel-based modeling.
- We propose a novel model MoSE, which integrates a newly designed subgraph extraction strategy based on anonymous walks with a mixture of learnable subgraph experts guided by a subgraph-aware gating mechanism. Grounded in the Subgraph Weisfeiler-Lehman (SWL) test, the model captures discriminative subgraph patterns.
- Extensive experiments across 19 datasets on both graph-level and node-level tasks demonstrate the superiority, efficiency, and interpretability of our model over other competitive baselines.

## Preliminaries

### Notation and Problem Formulation

Let  $G = (\mathcal{V}, \mathcal{E})$  denote an undirected, unweighted graph, where  $\mathcal{V} = \{v_1, v_2, \dots, v_n\}$  is the set of  $n$  nodes and  $\mathcal{E} \subseteq \mathcal{V} \times \mathcal{V}$  represents the edge set, respectively. The topological structure of  $G$  can also be represented by a binary adjacency matrix  $\mathbf{A} \in \mathbb{R}^{n \times n}$ , where  $\mathbf{A}_{ij} = 1$  iff the nodes  $v_i$  and  $v_j$  are connected, otherwise  $\mathbf{A}_{ij} = 0$ . Given a node  $u \in \mathcal{V}$ , denote its neighbors as  $\mathcal{N}(u) := \{v \in \mathcal{V} : \{u, v\} \in \mathcal{E}\}$ . We denote the node attributes/features as a matrix  $\mathbf{X} \in \mathbb{R}^{n \times f}$  where  $f$  is the feature dimension.  $\mathbf{Y}$  is denoted as the node/graph label set, and each node/graph is assigned to a label  $y \in \mathbf{Y} = \{1, 2, \dots, C\}$ , where  $C$  is the number of total classes for node/graph classification task.

In this paper, we focus on two fundamental graph learning tasks: node classification and graph classification. The goal is to learn a representation function that maps each node or an entire graph to a low-dimensional embedding space, such that the learned representations can support accurate downstream classification.

### Random Walk Kernel

Random walk kernel (RWK) was originally proposed (Gärtner, Flach, and Wrobel 2003; Kashima, Tsuda, and Inokuchi 2003) to measure the similarity between two graphs by counting the number of walks they share. To efficiently compute such walk-based similarity, RWK introduces the concept of direct product graph as follows:

**Definition 1 (Direct Product Graph).** *Given two graphs  $G = (\mathcal{V}, \mathcal{E})$  and  $G' = (\mathcal{V}', \mathcal{E}')$ , their direct product graph  $G_{\times} = (\mathcal{V}_{\times}, \mathcal{E}_{\times})$  is a graph with vertices  $\mathcal{V}_{\times} = \{(v, v') : v \in \mathcal{V} \wedge v' \in \mathcal{V}'\}$  and edges  $\mathcal{E}_{\times} = \{\{(u, u'), (v, v')\} : \{u, v\} \in \mathcal{E} \wedge \{u', v'\} \in \mathcal{E}'\}$ .*

It is obvious that  $G_{\times}$  is a graph over pairs of nodes from  $G$  and  $G'$ , and two nodes in  $G_{\times}$  are neighbors if and only if the corresponding nodes in  $G$  and  $G'$  are both neighbors. Therefore, performing a random walk on  $G_{\times}$  is equivalent to performing simultaneous random walks on  $G$  and  $G'$ . Given step  $P \in \mathbb{N}$ , the  $P$ -step random walk kernel between two graphs  $G$  and  $G'$  is defined as:

$$\mathcal{K}(G, G') = \sum_{p=0}^P \mathcal{K}^{(p)}(G, G') = \sum_{p=0}^P \sum_{i=1}^{|\mathcal{V}_{\times}|} \sum_{j=1}^{|\mathcal{V}_{\times}|} \lambda_p [\mathbf{A}_{\times}^p]_{ij}, \quad (1)$$

where  $\mathbf{A}_{\times}$  is the adjacency matrix of  $G_{\times}$  and  $\lambda = (\lambda_0, \lambda_1, \dots, \lambda_P)$  is a sequence of weights. Note that the  $(i, j)$ -th entry of  $\mathbf{A}_{\times}^p$  (i.e.,  $\mathbf{A}_{\times}$  to the power  $p$ ) is the number of common walks of step length  $p$  between the  $i$ -th and  $j$ -th node in  $G_{\times}$ .

To enable integration with neural networks, RWK is extended from the discrete formulation to a continuous version. Let  $\mathbf{S} = \mathbf{X}' \mathbf{X}^{\top} \in \mathbb{R}^{n' \times n}$  be the dot product similarity between the node attributes from two graphs, and we flatten  $\mathbf{S}$  into a vector  $\mathbf{s} := \text{vec}(\mathbf{S}) \in \mathbb{R}^{nn'}$  for notational convenience. The differentiable version of Eq. (1) can then be reformulated as:

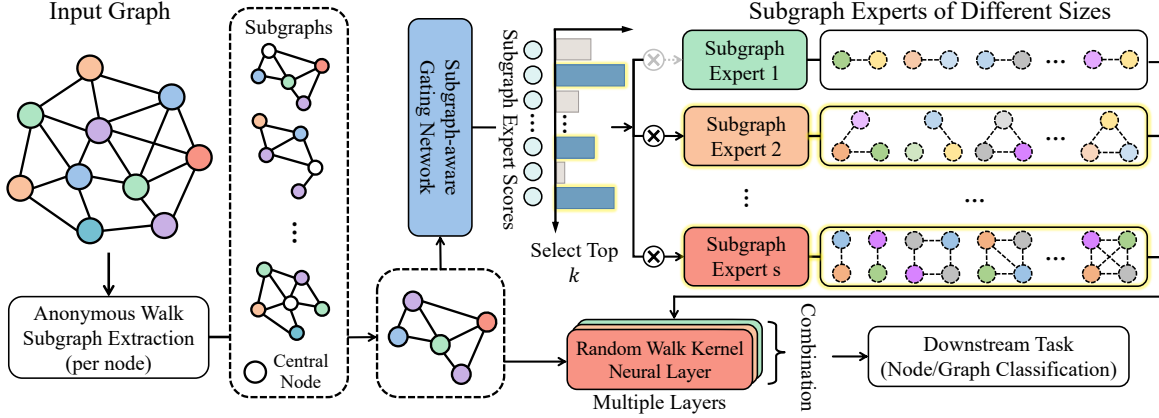


Figure 2: The overall architecture of MoSE. The subgraph of each node is extracted via anonymous walks and is routed to suitable subgraph experts (highlighted in yellow) through a subgraph-aware gating network.

$$\mathcal{K}^{(p)}(G, G') = \sum_{i=1}^{|V_x|} \sum_{j=1}^{|V_x|} \mathbf{s}_i \mathbf{s}_j [\mathbf{A}_x^p]_{ij} = \mathbf{s}^\top \mathbf{A}_x^p \mathbf{s}, \quad (2)$$

which facilitates end-to-end learning.

### Random Walk Kernel Neural Network

Building on the differentiable formulation of the RWK, recent works have proposed random walk kernel neural networks (Nikolentzos and Vazirgiannis 2020; Lee, Zhao, and Akoglu 2024), which integrate RWK into end-to-end trainable architectures. These models adopt a set of trainable hidden graphs  $H_i$  in each layer as structural probes and encode the input graph  $G$  by computing its similarity with each hidden graph via the Eq. (2). Formally, the graph-level representation of  $G$  is obtained as a concatenation of its RWK-based similarities with all hidden graphs:

$$\mathbf{h}(G) = \big\|_{i=1}^k \mathcal{K}^{(p)}(G, H_i) = \left[ \mathcal{K}^{(p)}(G, H_1), \dots, \mathcal{K}^{(p)}(G, H_k) \right], \quad (3)$$

where  $\|$  is the concatenation operator. The graph representation  $\mathbf{h}(G)$  is then fed into a classifier for prediction.

## Proposed Method

This section details our proposed method named MoSE which consists of three key components: a new subgraph extraction strategy, topology-aware expert routing, and subgraph experts. The overall framework is shown in Fig. 2.

### Anonymous Walk-based Subgraph Extraction

For subgraph-based graph learning methods, the subgraph extraction plays a crucial role in determining the expressiveness of the model (Zeng et al. 2023), as the extracted subgraphs define the local context within the node. The most widely adopted strategy is the  $h$ -hop induced ego graph of node  $v$ , denoted as  $\mathcal{B}(v, h)$ . Many practical implementations

restrict themselves to  $\mathcal{B}(v, 1)$  since the number of nodes grows exponentially with increasing  $h$ , leading to substantial computational overhead. Unfortunately,  $\mathcal{B}(v, 1)$  is often insufficient for capturing long-range dependencies. To address these limitations, we consider using anonymous walks (Ivanov and Burnaev 2018), a compact yet expressive descriptor, as the basis for subgraph extraction. Unlike random walks, anonymous walks ignore node identities and focus on structure, better capturing frequent subgraph patterns.

**Definition 2 (Anonymous Walk).** Given a random walk  $w = (v_0, v_1, \dots, v_L)$  on a graph, the corresponding anonymous walk is defined as a sequence of integers  $a = (\gamma_0, \gamma_1, \dots, \gamma_L)$ , where  $\gamma_i = \min \text{pos}(w, v_i)$ , and  $\text{pos}(w, v_i)$  returns the position at which the node  $v_i$  first appears in the walk  $w$ . We denote the mapping of a random walk  $w$  to the anonymous walk  $a$  by  $w \mapsto a$ .

**Proposition 1.** Let  $G = (\mathcal{V}, \mathcal{E})$  be a graph and  $v \in \mathcal{V}$ . A sufficiently rich distribution  $\mathcal{D}_l$  over length- $l$  anonymous walks starting at  $v$  with  $l = \mathcal{O}(|\mathcal{E}'|)$ , is sufficient to reconstruct the ego graph  $\mathcal{B}(v, h) = (\mathcal{V}', \mathcal{E}')$  centered at  $v$  with radius  $h$ .

Prop. 3 follows from Theorem 1 in (Micali and Zhu 2016). It shows that the distribution of anonymous walks rooted at a node contains sufficient information to reconstruct the ego graph around that node within a fixed radius. This motivates us to extract subgraphs by selecting representative anonymous walk patterns instead of relying on  $h$ -hop ego graph.

We begin by sampling random walks of fixed length starting from the node  $v$ . The resulting walk set is denoted as  $\mathcal{W}_v$ . Each walk is then mapped to its anonymous walk, forming the set as:

$$\mathcal{A}_v = \{w \mapsto a : w \in \mathcal{W}_v\}. \quad (4)$$

Next, we aggregate all anonymous walks from all nodes and identify the most frequently occurring patterns in the graph. Let  $k_{\text{walk}}$  be the number of walk patterns to retain. The global top- $k_{\text{walk}}$  anonymous walk patterns are defined as follows:

$$\mathcal{P} = \text{TopK} \left( \bigcup_{v \in \mathcal{V}} \mathcal{A}_v, k_{\text{walk}} \right). \quad (5)$$

For each node  $v$ , we collect all nodes that appear in random walks whose corresponding anonymous walk belongs to the top patterns  $\mathcal{P}$ . These nodes form the anonymous walk-based neighborhood  $\mathcal{N}_v^{aw}$ . Finally, we induce the subgraph  $G_v$  from the original graph using node  $v$  and  $\mathcal{N}_v^{aw}$ :

$$G_v = G[\{v\} \cup \mathcal{N}_v^{aw}]. \quad (6)$$

### Subgraph-aware Gating Network

Once the subgraph  $G_v = (\mathcal{V}_v, \mathcal{E}_v)$  is extracted for each node  $v$ , we proceed to assign it to the most appropriate experts. However, existing noisy gating mechanisms (Shazeer et al. 2017; Zhang et al. 2025) typically ignore the underlying graph topology. To address this limitation, we propose a subgraph-aware gating network that conditions expert selection on the topology-aware subgraph  $G_v$  as follows:

$$\boldsymbol{\eta}(v) = \sigma \left( \mathbf{x}_v + \sum_{u \in \mathcal{V}_v} \alpha_{uv} \mathbf{x}_u \right), \quad (7)$$

$$\boldsymbol{\psi}(v) = \boldsymbol{\eta}(v) \mathbf{W}_g + \epsilon \cdot \text{Softplus}(\boldsymbol{\eta}(v) \mathbf{W}_n), \quad (8)$$

$$\boldsymbol{\zeta}(v) = \text{Softmax}(\text{TopK}(\boldsymbol{\psi}(v), k_{ept})), \quad (9)$$

where  $\alpha_{uv} = \exp(\mathbf{x}_u^\top \mathbf{x}_v) / \sum_{u \in \mathcal{V}_v} \exp(\mathbf{x}_u^\top \mathbf{x}_v)$  are non-parametric attention weights, and  $\sigma(\cdot)$  is a nonlinear activation function. The matrices  $\mathbf{W}_g, \mathbf{W}_n \in \mathbb{R}^{f \times K}$  are trainable parameters that respectively produce clean and noisy scores, with  $\epsilon \in \mathcal{N}(0, 1)$  denoting the standard Gaussian noise. The resulting  $\boldsymbol{\psi}(v) \in \mathbb{R}^K$  are pre-selection logits over all  $K$  experts, and  $\boldsymbol{\zeta}(v) \in \mathbb{R}^{k_{ept}} = [E_1^v, E_2^v, \dots, E_{k_{ept}}^v]$  denotes the final sparse routing weights over the top- $k_{ept}$  selected experts.

### Subgraph Experts

Having selected the proper experts for each node  $v$ , we now introduce the architecture of each expert and describe how they process the subgraph  $G_v$ .

We define a group of  $K$  experts as  $E = \{E_s : s = 1, 2, \dots, K\}$  where each expert  $E_s$  consists of  $N$  hidden graphs of size  $s$ , denoted as  $E_s = \{H_1^s, H_2^s, \dots, H_N^s\}$ . Each hidden graph  $H_i^s$  is equipped with a learnable adjacency matrix  $\text{ReLU}(\mathbf{W}_i) \in \mathbb{R}^{s \times s}$  and a learnable feature matrix  $\mathbf{Z}_i \in \mathbb{R}^{s \times f}$ .

Given a node  $v$  and its extracted subgraph  $G_v$  with the corresponding adjacency matrix and node features  $\mathbf{A}_{G_v}$  and  $\mathbf{X}_{G_v}$ , each expert computes the node representation through  $N$  hidden graphs as:

$$\mathbf{h}_s(v) = \text{MLP} \left( \left\| \begin{array}{c} \mathcal{K}^{(p)}(G_v, H_i^s) \end{array} \right\|_{i=1}^N \right), \quad (10)$$

where  $\mathcal{K}^{(p)}(G_v, H_i^s)$  represents the  $p$ -step random walk kernel between  $G_v$  and  $H_i^s$ , computed as follows:

$$\begin{aligned} \mathcal{K}^{(p)}(G_v, H_i^s) &= \mathbf{s}^\top (\mathbf{A}_{G_v}^p \otimes \text{ReLU}(\mathbf{W}_i)^p) \mathbf{s} \\ &= \mathbf{s}^\top \text{vec}(\text{ReLU}(\mathbf{W}_i)^p) \text{vec}^{-1}(\mathbf{s}) \mathbf{A}_{G_v}^p \\ &= \mathbf{1}^\top [\mathbf{Z}_i \mathbf{X}_{G_v}^\top \odot \text{ReLU}(\mathbf{W}_i)^p \mathbf{Z}_i \mathbf{X}_{G_v}^\top \mathbf{A}_{G_v}^p] \mathbf{1}. \end{aligned} \quad (11)$$

After obtaining the expert-specific node representation  $\mathbf{h}_s(v)$ , we combine them into a final representation for node  $v$  based on the routing weights  $\boldsymbol{\zeta}(v)$  produced by Eq. (9). Specifically, the final representation is computed as:

$$\mathbf{h}(v) = \text{COMB}(\{\mathbf{h}_s(v) : s \in \mathcal{M}\}, \boldsymbol{\zeta}(v)), \quad (12)$$

where  $\mathcal{M}$  denotes the set of selected expert indices and  $\text{COMB}(\cdot)$  can either be a weighted sum  $\sum_{m \in \mathcal{M}} E_m^v \mathbf{h}_m(v)$  or concatenation form  $\text{MLP}(\left\|_{m \in \mathcal{M}} E_m^v \mathbf{h}_m(v)\right\|)$ .

For graph-level tasks, we apply a readout function over all node embeddings:

$$\mathbf{h}(G) = \text{READOUT}(\{\mathbf{h}(v) | v \in \mathcal{V}\}), \quad (13)$$

where  $\text{READOUT}(\cdot)$  is a permutation-invariant pooling.

### Optimization Objective

Following classic MoE works (Shazeer et al. 2017; Wang et al. 2023; Zhang et al. 2025), to prevent the gating network from consistently selecting a few experts, causing expert load imbalance during the training process, we introduce an expert importance loss as:

$$\text{Importance}(\mathcal{V}) = \sum_{v \in \mathcal{V}} \sum_{m \in \mathcal{M}} E_m^v, \quad (14)$$

$$\mathcal{L}_{\text{importance}}(\mathcal{V}) = \text{CV}(\text{Importance}(\mathcal{V}))^2, \quad (15)$$

where  $\text{Importance}(\mathcal{V})$  represents the sum of each node's expert scores across all nodes,  $\text{CV}(\cdot)$  denotes the coefficient of variation, which encourages a more uniform positive distribution. Therefore,  $\mathcal{L}_{\text{importance}}$  discourages expert collapse by minimizing disparity. The final loss function combines both task-specific loss and expert balance loss as follows:

$$\mathcal{L} = \mathcal{L}_{\text{task}} + \beta \cdot \mathcal{L}_{\text{importance}}, \quad (16)$$

where  $\beta$  is a hyperparameter controlling the trade-off between two losses.

### Theoretical Analysis

In this section, we analyze the expressive power of MoSE from the aspect of Subgraph Weisfeiler-Lehman Test (Zhang et al. 2023; Zhao et al. 2022) and the computational complexity of the proposed model.

### Expressive Power of MoSE

To motivate our analysis, we begin by reviewing the classical 1-WL test and its subgraph-based generalization.

**Definition 3 (1-WL Node Refinement).** Let  $G = (\mathcal{V}, \mathcal{E})$  be a graph, and let  $c_v^{(0)}$  denote the initial color (label) of node  $v$ . At each iteration  $t \geq 0$ , the 1-WL test updates the node color by aggregating the multiset of neighbor colors:

$$c_v^{(t+1)} = \text{hash} \left( c_v^{(t)}, \left\{ c_u^{(t)} \mid u \in \mathcal{N}(v) \right\} \right).$$

After  $T$  iterations, the multiset  $\left\{ c_v^{(T)} \mid v \in \mathcal{V} \right\}$  serves as the graph's fingerprint. Two graphs are distinguished if their fingerprints differ.

Modern MPNNs are known to be bounded by 1-WL (Morris et al. 2019), which limits their ability to distinguish certain non-isomorphic graphs. This is due to the fact that 1-WL only aggregates neighborhood color multisets without considering the structural relations among neighbors. To enhance discrimination, SWL replaces the 1-hop neighborhood multiset with a richer subgraph view as follows:

**Definition 4 (SWL Node Refinement).** *Subgraph Weifeiler-Lehman generalizes the 1-WL graph isomorphism test algorithm by replacing the color refinement at iteration  $t$  with  $c_v^{(t+1)} = \text{hash}(G_v^{(t)})$ , where  $G_v^{(t)} = (\mathcal{V}_v, \mathcal{E}_v, c_v^{(t)})$  is the induced subgraph rooted at node  $v$ .*

In MoSE, each node  $v$  is first associated with a topology-aware subgraph  $G_v$  extracted via anonymous walk-based policy. Then, the model computes a vector  $\Phi(G_v) := [\mathcal{K}^{(p)}(G_v, H_i)]_{i=1}^N$  of random walk kernel similarities between  $G_v$  and a set of learnable hidden graphs  $\{H_i\}_{i=1}^N$ , followed by an injective MLP mapping. This operation can be interpreted as a learned hashing mechanism applied to  $G_v$ :

$$c_v^{(t+1)} = \rho(\Phi(G_v)) = \rho\left(\left[\mathcal{K}^{(p)}(G_v, H_i)\right]_{i=1}^N\right),$$

where  $\rho$  is the MLP. To make this statement precise, we establish the following proposition and further give our corollary.

**Proposition 2.** *Let  $\mathcal{H} = \{H_i\}_{i=1}^N$  be a sufficiently large set of hidden graphs, and let  $\mathcal{K}^{(p)}$  be a positive-definite random walk kernel that distinguishes all non-isomorphic subgraphs of bounded size. If  $\rho$  is injective, then the representation  $c_v^{(t+1)}$  computed by MoSE is injective over the set of  $G_v$ , i.e., MoSE simulates one round of SWL node refinement.*

**Corollary 1.** *Let  $G$  and  $G'$  be two graphs, and let  $\pi$  denote a fixed subgraph extraction policy. If the SWL test distinguishes  $G$  and  $G'$  under policy  $\pi$ , then MoSE also distinguishes  $G$  and  $G'$  under the same policy, provided the conditions in Prop. 4 hold.*

Cor. 2 shows that the expressiveness of MoSE is more powerful than SWL. The proof of Prop. 4 and Cor. 2 is given in Appendix A.2 and A.3.

## Complexity Analysis

The complexity of MoSE consists of two main parts: anonymous walk-based subgraph extraction, and random walk kernel with hidden graphs. We denote the set of anonymous walks of length  $l$  starting from node  $v$  in graph  $G$  as  $\Omega^l(G, v)$ , therefore, the complexity for sampling anonymous walks is  $\mathcal{O}(nl \cdot |\Omega^l(G, v)|)$  where  $n$  is the total number of nodes. For computing the RWK in Eq. (11), since the adjacency matrix is stored as a sparse matrix with  $m$  non-zero entries, each subgraph expert calculation takes a computation time of  $\mathcal{O}(Pf(\bar{N}s(s+n) + m))$ , where  $P$  is the maximum length of random walks,  $f$  is the feature dimension,  $\bar{N}$  is hidden graphs number, and  $s$  is the hidden graph size. The training procedure of MoSE is given in Appendix B.1.

## Experiments

We conduct comprehensive experiments to validate the effectiveness and generalization of MoSE. The ablation study is then given to help us better understand our model.

### Experiment Settings

**Datasets.** We conduct experiments on both graph-level and node-level tasks across a wide range of graph datasets. Their details and statistics are presented in Appendix B.2.

- **Graph Classification:** We choose both real-world and synthetic graph datasets to evaluate our model. For the real-world ones, we use 8 publicly available graph classification datasets, including 5 biological and chemical compounds: MUTAG (Debnath et al. 1991), D&D (Dobson and Doig 2003), NCI1 (Wale, Watson, and Karypis 2008), PROTEINS, ENZYMES (Borgwardt et al. 2005), and 3 social interaction datasets: IMDB-BINARY, IMDB-MULTI, and REDDIT-BINARY (Yarardag and Vishwanathan 2015). For the synthetic ones, we include GraphFive and GraphCycle. GraphFive consists of five local structure classes: caveman, cycle, grid, ladder, and star. GraphCycle consists of two classes: Cycle and Non-Cycle.

- **Node Classification:** We choose 9 widely used node classification benchmarks, including 3 homophilic and 6 heterophilic graphs. We choose the most common citation networks (Kipf and Welling 2017): Cora, Citeseer, and Pubmed as our homophilic datasets. We consider Wikipedia networks (Chameleon and Squirrel), Actor co-occurrence network (Actor), and WebKB (Cornell, Texas, and Wisconsin) (Pei et al. 2020) as heterophilic datasets.

**Compared Methods.** We compare the proposed model with the following baselines, which can be categorized into three categories: (1) Graph kernel methods: graphlet kernel (GL) (Sherashidze et al. 2009), shortest path kernel (SP) (Borgwardt and Kriegel 2005) and Weisfeiler-Lehman subtree kernel (WL) (Shervashidze et al. 2011). (2) widely used MPNN-based GNNs: GCN (Kipf and Welling 2017), GAT (Veličković et al. 2018), GIN (Xu et al. 2019), and GraphSAGE (Hamilton, Ying, and Leskovec 2017). (3) Graph kernel-based GNNs: RWNN (Nikolentzos and Vazirgiannis 2020), KerGNN (Feng et al. 2022), GNN-AK (Zhao et al. 2022), RWK<sup>+</sup>CN (Lee, Zhao, and Akoglu 2024), GIP (Wang et al. 2024), GKNN (Cosmo et al. 2024).

**Setup.** To make a fair comparison with other baselines, for graph classification datasets, we follow the 10-fold cross-validation for model assessment and use the same splits as described in (Errica et al. 2020). For node classification datasets, we use the public splits for homophilous graphs, and each heterophilous graph is split into 60%/20%/20% for training, validation, and testing, respectively. The implementation details are presented in Appendix B.3.

### Performance Evaluation

**Graph Classification.** The graph classification results on real-world and synthetic graph datasets are shown in

Table 1: Graph classification accuracies and deviations (%  $\pm$  std) of the proposed model and the baselines on 8 real-world graph datasets. The best results are in **bold** and the second-best results are underlined.

Methods	MUTAG	D&D	NCI1	PROTEINS	ENZYMES	IMDB-BINARY	IMDB-MULTI	REDDIT-BINARY
GK	GL	80.8 $\pm$ 6.4	75.4 $\pm$ 3.4	61.8 $\pm$ 1.7	71.6 $\pm$ 3.1	25.1 $\pm$ 4.4	63.3 $\pm$ 2.7	39.6 $\pm$ 3.0
	SP	80.2 $\pm$ 6.5	78.3 $\pm$ 4.0	66.3 $\pm$ 2.6	71.9 $\pm$ 6.1	38.3 $\pm$ 8.0	57.5 $\pm$ 5.4	40.5 $\pm$ 2.8
	WL	84.6 $\pm$ 8.3	78.1 $\pm$ 2.4	<b>84.8 <math>\pm</math> 2.5</b>	73.8 $\pm$ 4.4	50.3 $\pm$ 5.7	72.8 $\pm$ 4.5	51.2 $\pm$ 6.5
MPNN	GCN	74.3 $\pm$ 8.1	72.1 $\pm$ 0.3	80.2 $\pm$ 2.0	75.5 $\pm$ 1.6	57.8 $\pm$ 0.7	<u>74.0 <math>\pm</math> 3.4</u>	51.9 $\pm$ 3.8
	GAT	86.4 $\pm$ 5.7	73.1 $\pm$ 3.4	82.4 $\pm$ 1.1	76.8 $\pm$ 1.7	<u>62.5 <math>\pm</math> 6.1</u>	72.0 $\pm$ 2.7	43.5 $\pm$ 3.5
	GIN	84.7 $\pm$ 6.7	75.3 $\pm$ 2.9	80.0 $\pm$ 1.4	73.3 $\pm$ 4.0	59.6 $\pm$ 4.5	71.2 $\pm$ 3.9	48.5 $\pm$ 3.3
	SAGE	83.6 $\pm$ 9.6	72.9 $\pm$ 2.0	76.0 $\pm$ 1.8	73.0 $\pm$ 4.5	58.2 $\pm$ 6.0	68.8 $\pm$ 4.5	47.6 $\pm$ 3.5
GK-based NN	RWNN	88.1 $\pm$ 4.8	76.9 $\pm$ 4.6	73.2 $\pm$ 2.0	74.1 $\pm$ 2.8	57.4 $\pm$ 4.9	70.6 $\pm$ 4.4	48.8 $\pm$ 2.9
	KerGNN	72.7 $\pm$ 0.9	78.9 $\pm$ 3.5	76.3 $\pm$ 2.6	75.5 $\pm$ 4.6	55.0 $\pm$ 5.0	73.7 $\pm$ 4.0	50.9 $\pm$ 5.1
	GNN-AK	91.3 $\pm$ 7.0	80.3 $\pm$ 0.7	79.1 $\pm$ 2.0	<u>77.1 <math>\pm</math> 5.7</u>	<b>62.5 <math>\pm</math> 1.8</b>	68.8 $\pm$ 3.2	44.5 $\pm$ 1.3
	RWK <sup>+</sup> CN	83.0 $\pm$ 6.4	74.8 $\pm$ 2.4	72.3 $\pm$ 1.3	76.2 $\pm$ 1.2	44.0 $\pm$ 2.7	71.6 $\pm$ 1.0	49.2 $\pm$ 0.6
	GIP	92.1 $\pm$ 3.3	79.5 $\pm$ 0.5	75.2 $\pm$ 1.5	76.8 $\pm$ 1.8	60.7 $\pm$ 2.6	71.1 $\pm$ 2.0	41.7 $\pm$ 1.5
	GKNN-GL	85.2 $\pm$ 2.3	78.6 $\pm$ 2.6	71.5 $\pm$ 1.2	75.4 $\pm$ 1.1	58.7 $\pm$ 3.2	69.9 $\pm$ 1.4	45.7 $\pm$ 1.2
	GKNN-WL	85.7 $\pm$ 2.8	81.2 $\pm$ 2.5	73.6 $\pm$ 1.3	74.9 $\pm$ 1.1	59.0 $\pm$ 2.6	69.7 $\pm$ 2.2	47.9 $\pm$ 1.8
MoSE	<b>92.7 <math>\pm</math> 2.5</b>	<b>83.7 <math>\pm</math> 1.6</b>	<u>83.7 <math>\pm</math> 1.7</u>	<b>78.6 <math>\pm</math> 4.4</b>	<b>62.5 <math>\pm</math> 1.8</b>	<b>83.0 <math>\pm</math> 3.2</b>	<b>52.6 <math>\pm</math> 1.1</b>	<b>92.1 <math>\pm</math> 1.4</b>

Table 2: Graph classification accuracies and F1 scores (%  $\pm$  std) on synthetic datasets. The best results are in **bold** and the second-best results are underlined.

Datasets $\rightarrow$ Methods $\downarrow$	GraphFive		GraphCycle	
	Acc.	F1	Acc.	F1
SP	56.7 $\pm$ 1.3	52.6 $\pm$ 1.0	79.8 $\pm$ 1.0	73.5 $\pm$ 0.9
WL	60.1 $\pm$ 0.4	<u>56.3 <math>\pm</math> 0.3</u>	81.1 $\pm$ 0.8	76.4 $\pm$ 0.8
GCN	59.0 $\pm$ 2.3	53.8 $\pm$ 0.9	81.2 $\pm$ 1.1	73.0 $\pm$ 1.0
SAGE	59.5 $\pm$ 0.5	51.2 $\pm$ 0.5	79.8 $\pm$ 1.1	71.2 $\pm$ 2.6
RWNN	58.8 $\pm$ 1.5	53.7 $\pm$ 1.0	80.5 $\pm$ 1.7	<u>78.5 <math>\pm</math> 2.8</u>
KerGNN	57.9 $\pm$ 0.5	49.7 $\pm$ 0.1	79.3 $\pm$ 0.8	71.8 $\pm$ 0.6
GIP	60.4 $\pm$ 1.8	55.9 $\pm$ 2.5	<b>82.5 <math>\pm</math> 1.2</b>	77.9 $\pm$ 5.7
MoSE	<b>62.3 <math>\pm</math> 1.2</b>	<b>57.4 <math>\pm</math> 0.9</b>	<u>82.3 <math>\pm</math> 1.8</u>	<b>78.7 <math>\pm</math> 0.8</b>

Tab. 1 and Tab. 2, respectively. We observe that traditional graph kernels remain competitive, occasionally even outperforming MPNN-based GNNs on datasets with relatively small average graph sizes, such as MUTAG, NCI1, IMDB-BINARY, and IMDB-MULTI. However, on datasets with larger average numbers of nodes, MPNN-based models exhibit advantages in both classification accuracy and performance stability. Meanwhile, GK-based GNNs inherit the expressive power of classical graph kernels and thus achieve strong overall performance on graph classification benchmarks. A similar trend can also be found on the synthetic datasets, further supporting the generality of these findings. Among GK-based GNNs, MoSE consistently achieves the best or near-best results over 10 real-world and synthetic graph datasets. We attribute this to the MoE design, which enables our model to dynamically select and integrate informative subgraphs, effectively capturing diverse local patterns in different types of graphs.

**Node Classification.** The node classification results are shown in Tab. 3. We find that MPNN models generally perform well in homophilous graphs, where neighboring nodes

are likely to share the same label. However, their performance tends to degrade under heterophily, where aggregating features from neighbors with different labels may dilute the target node's embedding. Conversely, GK-based models often perform better in heterophilous graphs, where the local structural patterns provide useful discriminative signals beyond label similarity. With the help of MoE design, our model significantly improves upon GK-based GNNs in both scenarios. Especially on heterophilous graphs, MoSE further amplifies the advantages of GK-based approaches.

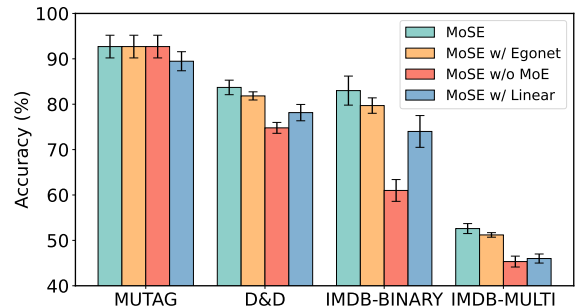


Figure 3: Ablation study with different MoSE variants.

### Ablation Study and Visualization

To better understand the contribution of each component in our model, we conduct ablation studies on several variants of MoSE. Specifically, we examine the effect of the subgraph extraction strategy, removing the MoE mechanism, and substituting the gating with a linear one. The results are shown in Fig. 3. Due to the small size of MUTAG, only the gating mechanism produces a noticeable performance difference. On other datasets, we find that the MoE component has the largest impact on performance, confirming its importance for capturing diverse subgraph semantics. Furthermore, subgraph-aware gating also contributes significantly

Table 3: Node classification accuracies on real-world graph datasets ( $\% \pm \text{std}$ ). The best results are in **bold** and the second-best results are underlined. - means Out of Resources, either time or GPU memory.

Methods	Cora	Citeseer	Pubmed	Chameleon	Squirrel	Actor	Cornell	Texas	Wisconsin	
MPNN	GCN	$80.8 \pm 0.5$	$70.8 \pm 0.5$	$79.0 \pm 0.3$	$59.8 \pm 2.6$	$36.9 \pm 1.3$	$30.3 \pm 0.8$	$53.8 \pm 8.6$	$54.1 \pm 4.4$	$50.4 \pm 7.6$
	GAT	$83.0 \pm 0.7$	$71.9 \pm 1.4$	$85.3 \pm 0.6$	$54.7 \pm 2.0$	$30.6 \pm 2.1$	$27.4 \pm 0.9$	$55.0 \pm 5.6$	$52.2 \pm 6.6$	$54.3 \pm 5.6$
	GIN	$81.9 \pm 0.6$	$68.1 \pm 0.6$	$85.7 \pm 0.3$	$56.2 \pm 1.9$	$35.8 \pm 1.3$	$23.6 \pm 0.8$	$38.7 \pm 5.2$	$29.0 \pm 4.4$	$45.7 \pm 4.7$
	SAGE	<b><math>87.7 \pm 1.8</math></b>	<u><math>76.7 \pm 0.6</math></u>	<b><math>87.1 \pm 0.7</math></b>	$55.1 \pm 1.8$	$39.8 \pm 1.9$	$24.2 \pm 1.4$	$71.0 \pm 4.8$	$67.4 \pm 3.1$	$73.9 \pm 6.8$
GK-based NN	RWNN	$71.8 \pm 2.1$	$68.9 \pm 0.5$	$64.6 \pm 0.3$	$46.3 \pm 2.7$	$29.8 \pm 2.4$	$34.1 \pm 0.3$	$62.8 \pm 5.2$	$61.5 \pm 7.5$	$75.4 \pm 6.2$
	KerGNN	$72.9 \pm 0.7$	$70.3 \pm 0.4$	$68.1 \pm 0.2$	$48.2 \pm 2.5$	$33.9 \pm 1.6$	$34.6 \pm 0.4$	$64.9 \pm 3.9$	$79.9 \pm 7.1$	<u><math>87.5 \pm 4.6</math></u>
	GNN-AK	$58.9 \pm 0.3$	$50.1 \pm 1.6$	$73.8 \pm 0.6$	$56.8 \pm 1.1$	$34.5 \pm 1.1$	$35.8 \pm 2.4$	$72.4 \pm 1.4$	<u><math>83.2 \pm 1.6</math></u>	$84.3 \pm 2.0$
	RWK <sup>+</sup> CN	$72.5 \pm 1.7$	<b><math>76.7 \pm 0.2</math></b>	$68.9 \pm 0.5$	$47.4 \pm 1.3$	$35.1 \pm 1.6$	<u><math>36.0 \pm 0.2</math></u>	$72.3 \pm 3.1$	$69.4 \pm 6.0$	$73.5 \pm 2.4$
	GIP	$76.6 \pm 1.5$	$61.6 \pm 0.1$	$77.5 \pm 0.4$	<b><math>66.6 \pm 0.7</math></b>	<u><math>56.3 \pm 1.1</math></u>	$24.9 \pm 1.9$	$54.1 \pm 5.3$	$82.4 \pm 6.8$	$78.4 \pm 2.0$
	GKNN-GL	-	-	-	-	-	-	-	-	
	GKNN-WL	-	-	-	-	-	-	$54.1 \pm 0.1$	$54.1 \pm 0.0$	$49.2 \pm 1.0$
MoSE	<u><math>83.9 \pm 2.0</math></u>	$74.3 \pm 0.4$	$79.8 \pm 0.3$	<u><math>64.5 \pm 1.1</math></u>	<b><math>58.8 \pm 0.7</math></b>	<b><math>39.6 \pm 1.1</math></b>	<b><math>73.0 \pm 3.4</math></b>	<b><math>83.7 \pm 3.8</math></b>	<b><math>87.5 \pm 4.3</math></b>	

by enabling the model to better associate input subgraphs with suitable experts. Lastly, the anonymous walk-based subgraph extraction is capable of isolating more discriminative local patterns.

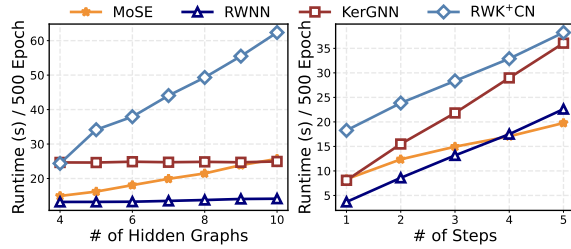


Figure 4: Running time comparison under different settings.

We also evaluate the time complexity of our model under different configurations. Fig. 4 reports the runtime per 500 epochs when varying the number of hidden graphs and RWK max steps, compared against other RWK-based models. The results show that the runtime of MoSE remains within a reasonable range, and scales smoothly with the number of steps. This confirms that our model offers an affordable trade-off between expressiveness and efficiency.

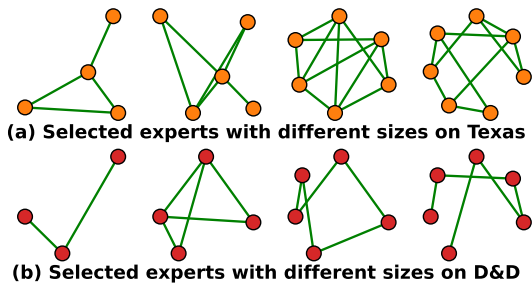


Figure 5: Subgraph experts visualization.

Furthermore, the visualization of the learned subgraph experts, presented in Fig. 5, showcases the diversity and inter-

pretability of our model. Compared to the case study in Introduction, our experts exhibit fewer redundant nodes while preserving key structural signals. The hyperparameter sensitivity analysis and additional visualizations on more datasets can be found in the Appendix B.4 and B.5.

## Related Work

**Hybrid Graph Kernels and GNNs.** Graph kernels and GNNs are both fundamental tools for graph learning. Graph kernels, rooted in classical machine learning, provide interpretability by measuring graph similarities. In contrast, GNNs excel at efficient message passing, enabling flexible and scalable representation learning. While many works have attempted to bridge graph kernels and GNNs, existing approaches can be categorized into two aspects: using GNNs to enhance or design kernels (Hazan and Jaakkola 2015; Du et al. 2019), and incorporating kernel principles into GNN design (Mairal 2016; Feng et al. 2022; Lee, Zhao, and Akoglu 2024; Chen, Jacob, and Mairal 2020). Our work falls into the second one, with a particular focus on integrating the widely used random walk kernel into GNNs to enhance their structural pattern awareness.

**Graph Mixture of Experts.** The Mixture of Experts (MoE) is a long-standing machine learning paradigm (Jordan and Jacobs 1993; Chen, Xu, and Chi 1999) that trains multiple specialized experts to cooperatively enhance training efficiency and model performance. While MoE has been widely used in fields such as large language models (Fedus, Zoph, and Shazeer 2022), video recognition (Li and Xu 2023), its application to graph remains relatively under-explored. Recently, a few pioneering efforts have extended MoE to the graph domain. GMoE (Wang et al. 2023) uses GNN with different hop numbers as experts to learn hop information. MoG (Zhang et al. 2025) incorporates multiple sparsifiers to personalize unique sparsity level and pruning criteria for each node. GraphMoRE (Guo et al. 2025) introduces diverse Riemannian experts to embed the graph into manifolds with varying curvatures. In graph fairness learning, G-Fame (Liu et al. 2023) is proposed as a plug-and-play

method to learn distinguishable embeddings with multiple experts capturing different aspects of knowledge.

## Conclusion

In this paper, we focus on subgraph pattern learning and propose MoSE framework for flexibility and adaptability across diverse graph tasks. By leveraging multiple subgraph experts with a newly designed subgraph extraction strategy and routing mechanism, our model captures meaningful local structures with controllable complexity. Extensive experimental results demonstrate that our model achieves a favorable balance between performance, efficiency, and interpretability.

## References

Al-Rfou, R.; Perozzi, B.; and Zelle, D. 2019. DDGK: Learning Graph Representations for Deep Divergence Graph Kernels. In *The World Wide Web Conference, WWW '19*, 37–48. New York, NY, USA: Association for Computing Machinery. ISBN 9781450366748.

Arvind, V.; Fuhlbütt, F.; Köbler, J.; and Verbitsky, O. 2019. On Weisfeiler-Leman Invariance: Subgraph Counts and Related Graph Properties. In *Fundamentals of Computation Theory: 22nd International Symposium, FCT 2019, Copenhagen, Denmark, August 12–14, 2019, Proceedings*, 111–125. Berlin, Heidelberg: Springer-Verlag. ISBN 978-3-030-25026-3.

Borgwardt, K.; and Kriegel, H. 2005. Shortest-path kernels on graphs. In *Fifth IEEE International Conference on Data Mining (ICDM'05)*, 8 pp.–.

Borgwardt, K. M.; Ong, C. S.; Schönauer, S.; Vishwanathan, S.; Smola, A. J.; and Kriegel, H.-P. 2005. Protein Function Prediction via Graph Kernels. *Bioinformatics*, 21(suppl\_1): i47–i56.

Chen, D.; Jacob, L.; and Mairal, J. 2020. Convolutional kernel networks for graph-structured data. In *International Conference on Machine Learning*.

Chen, K.; Xu, L.; and Chi, H. 1999. Improved learning algorithms for mixture of experts in multiclass classification. *Neural Networks*, 12(9): 1229–1252.

Chen, Z.; Chen, L.; Villar, S.; and Bruna, J. 2020. Can Graph Neural Networks Count Substructures? In Larochelle, H.; Ranzato, M.; Hadsell, R.; Balcan, M.; and Lin, H., eds., *Advances in Neural Information Processing Systems*, volume 33, 10383–10395. Curran Associates, Inc.

Cosmo, L.; Minello, G.; Bicciato, A.; Bronstein, M. M.; Rodolà, E.; Rossi, L.; and Torsello, A. 2024. Graph kernel neural networks. *IEEE transactions on neural networks and learning systems*.

Debnath, A. K.; de Compadre, R. L. L.; Debnath, G.; Shuster, A. J.; and Hansch, C. 1991. Structure-activity relationship of mutagenic aromatic and heteroaromatic nitro compounds. Correlation with molecular orbital energies and hydrophobicity. *Journal of medicinal chemistry*, 34 2: 786–97.

Defferrard, M.; Bresson, X.; and Vandergheynst, P. 2016. Convolutional Neural Networks on Graphs with Fast Localized Spectral Filtering. *Advances in neural information processing systems*, 29.

Dobson, P. D.; and Doig, A. J. 2003. Distinguishing Enzyme Structures from Non-enzymes Without Alignments. *Journal of Molecular Biology*, 330(4): 771–783.

Du, S. S.; Hou, K.; Póczos, B.; Salakhutdinov, R.; Wang, R.; and Xu, K. 2019. *Graph neural tangent kernel: fusing graph neural networks with graph kernels*. Red Hook, NY, USA: Curran Associates Inc.

Errica, F.; Poddar, M.; Bacciu, D.; and Micheli, A. 2020. A Fair Comparison of Graph Neural Networks for Graph Classification. In *International Conference on Learning Representations*.

Fedus, W.; Zoph, B.; and Shazeer, N. 2022. Switch Transformers: Scaling to Trillion Parameter Models with Simple and Efficient Sparsity. arXiv:2101.03961.

Feng, A.; You, C.; Wang, S.; and Tassiulas, L. 2022. KerGNNs: Interpretable Graph Neural Networks with Graph Kernels. *Proceedings of the AAAI Conference on Artificial Intelligence*, 36(6): 6614–6622.

Feng, J.; Kong, L.; Liu, H.; Tao, D.; Li, F.; Zhang, M.; and Chen, Y. 2023. Extending the Design Space of Graph Neural Networks by Rethinking Folklore Weisfeiler-Lehman. In *Thirty-seventh Conference on Neural Information Processing Systems*.

Gärtner, T.; Flach, P. A.; and Wrobel, S. 2003. On Graph Kernels: Hardness Results and Efficient Alternatives. In *Annual Conference Computational Learning Theory*.

Guo, Z.; Sun, Q.; Yuan, H.; Fu, X.; Zhou, M.; Gao, Y.; and Li, J. 2025. GraphMoRE: Mitigating Topological Heterogeneity via Mixture of Riemannian Experts. *Proceedings of the AAAI Conference on Artificial Intelligence*, 39(11): 11754–11762.

Hamilton, W.; Ying, Z.; and Leskovec, J. 2017. Inductive Representation Learning on Large Graphs. *Advances in neural information processing systems*, 30.

Hao, Z.; Lu, C.; Huang, Z.; Wang, H.; Hu, Z.; Liu, Q.; Chen, E.; and Lee, C. 2020. ASGN: An Active Semi-supervised Graph Neural Network for Molecular Property Prediction. In *Proceedings of the 26th ACM SIGKDD International Conference on Knowledge Discovery & Data Mining, KDD '20*, 731–752. New York, NY, USA: Association for Computing Machinery. ISBN 9781450379984.

Hazan, T.; and Jaakkola, T. 2015. Steps toward deep kernel methods from infinite neural networks. *arXiv preprint arXiv:1508.05133*.

Ivanov, S.; and Burnaev, E. 2018. Anonymous Walk Embeddings. In Dy, J.; and Krause, A., eds., *Proceedings of the 35th International Conference on Machine Learning*, volume 80 of *Proceedings of Machine Learning Research*, 2186–2195. PMLR.

Jordan, M.; and Jacobs, R. 1993. Hierarchical mixtures of experts and the EM algorithm. In *Proceedings of 1993 International Conference on Neural Networks (IJCNN-93-Nagoya, Japan)*, volume 2, 1339–1344 vol.2.

Kashima, H.; Tsuda, K.; and Inokuchi, A. 2003. Marginalized kernels between labeled graphs. In *Proceedings of the Twentieth International Conference on International Conference on Machine Learning*, ICML'03, 321–328. AAAI Press. ISBN 1577351894.

Kipf, T. N.; and Welling, M. 2017. Semi-Supervised Classification with Graph Convolutional Networks. In *International Conference on Learning Representations*.

Lee, M.-C.; Zhao, L.; and Akoglu, L. 2024. Descriptive Kernel Convolution Network with Improved Random Walk Kernel. In *Proceedings of the ACM Web Conference 2024*, WWW '24, 457–468. New York, NY, USA: Association for Computing Machinery. ISBN 9798400701719.

Lei, T.; Jin, W.; Barzilay, R.; and Jaakkola, T. 2017. Deriving Neural Architectures from Sequence and Graph Kernels. In Precup, D.; and Teh, Y. W., eds., *Proceedings of the 34th International Conference on Machine Learning*, volume 70 of *Proceedings of Machine Learning Research*, 2024–2033. PMLR.

Leman, A.; and Weisfeiler, B. 1968. A reduction of a graph to a canonical form and an algebra arising during this reduction. *Nauchno-Technicheskaya Informatsiya*, 2(9): 12–16.

Li, X.; and Xu, H. 2023. MEID: Mixture-of-Experts with Internal Distillation for Long-Tailed Video Recognition. *Proceedings of the AAAI Conference on Artificial Intelligence*, 37(2): 1451–1459.

Liao, N.; Mo, D.; Luo, S.; Li, X.; and Yin, P. 2022. SCARA: scalable graph neural networks with feature-oriented optimization. *Proc. VLDB Endow.*, 15(11): 3240–3248.

Liu, H.; Liao, N.; and Luo, S. 2025. SIGMA: An efficient heterophilous graph neural network with fast global aggregation. In *2025 IEEE 41st International Conference on Data Engineering (ICDE)*, 1924–1937. IEEE.

Liu, Z.; Zhang, C.; Tian, Y.; Zhang, E.; Huang, C.; Ye, Y.; and Zhang, C. 2023. Fair Graph Representation Learning via Diverse Mixture-of-Experts. In *Proceedings of the ACM Web Conference 2023*, WWW '23, 28–38. New York, NY, USA: Association for Computing Machinery. ISBN 9781450394161.

Long, Q.; Jin, Y.; Wu, Y.; and Song, G. 2021. Theoretically Improving Graph Neural Networks via Anonymous Walk Graph Kernels. In *Proceedings of the Web Conference 2021*, WWW '21, 1204–1214. New York, NY, USA: Association for Computing Machinery. ISBN 9781450383127.

Mairal, J. 2016. End-to-End Kernel Learning with Supervised Convolutional Kernel Networks. In Lee, D.; Sugiyama, M.; Luxburg, U.; Guyon, I.; and Garnett, R., eds., *Advances in Neural Information Processing Systems*, volume 29. Curran Associates, Inc.

Micali, S.; and Zhu, Z. A. 2016. Reconstructing Markov processes from independent and anonymous experiments. *Discrete Applied Mathematics*, 200: 108–122.

Morris, C.; Ritzert, M.; Fey, M.; Hamilton, W. L.; Lenssen, J. E.; Rattan, G.; and Grohe, M. 2019. Weisfeiler and leman go neural: higher-order graph neural networks. In *Proceedings of the Thirty-Third AAAI Conference on Artificial Intelligence and Thirty-First Innovative Applications of Artificial Intelligence Conference and Ninth AAAI Symposium on Educational Advances in Artificial Intelligence*, AAAI'19/IAAI'19/EAAI'19. AAAI Press. ISBN 978-1-57735-809-1.

Nikolentzos, G.; and Vazirgiannis, M. 2020. Random Walk Graph Neural Networks. In Larochelle, H.; Ranzato, M.; Hadsell, R.; Balcan, M.; and Lin, H., eds., *Advances in Neural Information Processing Systems*, volume 33, 16211–16222. Curran Associates, Inc.

Pei, H.; Wei, B.; Chang, K. C.-C.; Lei, Y.; and Yang, B. 2020. Geom-GCN: Geometric Graph Convolutional Networks. In *International Conference on Learning Representations*.

Rong, Y.; Bian, Y.; Xu, T.; Xie, W.; Wei, Y.; Huang, W.; and Huang, J. 2020. Self-supervised graph transformer on large-scale molecular data. In *Proceedings of the 34th International Conference on Neural Information Processing Systems*, NIPS '20. Red Hook, NY, USA: Curran Associates Inc. ISBN 9781713829546.

Shazeer, N.; Mirhoseini, A.; Maziarz, K.; Davis, A.; Le, Q.; Hinton, G.; and Dean, J. 2017. Outrageously Large Neural Networks: The Sparsely-Gated Mixture-of-Experts Layer. In *International Conference on Learning Representations*.

Sherashidze, N.; Vishwanathan, S.; Petri, T.; Mehlhorn, K.; and Borgwardt, K. 2009. Efficient Graphlet Kernels for Large Graph Comparison. *12th International Conference on Artificial Intelligence and Statistics (AISTATS)*, Society for Artificial Intelligence and Statistics, 488–495 (2009), 5.

Shervashidze, N.; Schweitzer, P.; van Leeuwen, E. J.; Mehlhorn, K.; and Borgwardt, K. M. 2011. Weisfeiler-Lehman Graph Kernels. *Journal of Machine Learning Research*, 12(77): 2539–2561.

Veličković, P.; Cucurull, G.; Casanova, A.; Romero, A.; Liò, P.; and Bengio, Y. 2018. Graph Attention Networks. In *International Conference on Learning Representations*.

Wale, N.; Watson, I. A.; and Karypis, G. 2008. Comparison of Descriptor Spaces for Chemical Compound Retrieval and Classification. *Knowledge and Information Systems*, 14(3): 347–375.

Wang, H.; Jiang, Z.; You, Y.; Han, Y.; Liu, G.; Srinivasa, J.; Kompella, R. R.; and Wang, Z. 2023. Graph Mixture of Experts: Learning on Large-Scale Graphs with Explicit Diversity Modeling. In *NeurIPS*.

Wang, Y.; Liu, S.; Zheng, T.; Chen, K.; and Song, M. 2024. Unveiling Global Interactive Patterns across Graphs: Towards Interpretable Graph Neural Networks. In *Proceedings of the 30th ACM SIGKDD Conference on Knowledge Discovery and Data Mining*, KDD '24, 3277–3288. New York, NY, USA: Association for Computing Machinery. ISBN 9798400704901.

Wu, S.; Sun, F.; Zhang, W.; Xie, X.; and Cui, B. 2022. Graph Neural Networks in Recommender Systems: A Survey. *ACM Comput. Surv.*, 55(5).

Xu, K.; Hu, W.; Leskovec, J.; and Jegelka, S. 2019. How Powerful are Graph Neural Networks? In *International Conference on Learning Representations*.

Yanardag, P.; and Vishwanathan, S. 2015. Deep Graph Kernels. In *Proceedings of the 21th ACM SIGKDD International Conference on Knowledge Discovery and Data Mining*, KDD '15, 1365–1374. New York, NY, USA: Association for Computing Machinery. ISBN 9781450336642.

Yang, Y.; Wu, L.; Wang, Z.; He, Z.; Hong, R.; and Wang, M. 2024. Graph Bottlenecked Social Recommendation. In *Proceedings of the 30th ACM SIGKDD Conference on Knowledge Discovery and Data Mining*, KDD '24, 3853–3862. New York, NY, USA: Association for Computing Machinery. ISBN 9798400704901.

Yu, J.; Yin, H.; Xia, X.; Chen, T.; Cui, L.; and Nguyen, Q. V. H. 2022. Are Graph Augmentations Necessary? Simple Graph Contrastive Learning for Recommendation. In *Proceedings of the 45th International ACM SIGIR Conference on Research and Development in Information Retrieval*, SIGIR '22, 1294–1303. New York, NY, USA: Association for Computing Machinery. ISBN 9781450387323.

Zeng, D.; Liu, W.; Chen, W.; Zhou, L.; Zhang, M.; and Qu, H. 2023. Substructure Aware Graph Neural Networks. *Proceedings of the AAAI Conference on Artificial Intelligence*, 37(9): 11129–11137.

Zhang, B.; Feng, G.; Du, Y.; He, D.; and Wang, L. 2023. A Complete Expressiveness Hierarchy for Subgraph GNNs via Subgraph Weisfeiler-Lehman Tests. In Krause, A.; Brunskill, E.; Cho, K.; Engelhardt, B.; Sabato, S.; and Scarlett, J., eds., *Proceedings of the 40th International Conference on Machine Learning*, volume 202 of *Proceedings of Machine Learning Research*, 41019–41077. PMLR.

Zhang, G.; Sun, X.; Yue, Y.; Jiang, C.; Wang, K.; Chen, T.; and Pan, S. 2025. Graph Sparsification via Mixture of Graphs. In *International Conference on Learning Representations*.

Zhao, L.; Jin, W.; Akoglu, L.; and Shah, N. 2022. From Stars to Subgraphs: Uplifting Any GNN with Local Structure Awareness. In *International Conference on Learning Representations*.

## Theoretical Analysis

### Proof of Proposition 1

Before we proceed with the proof, we first restate the relevant definition and proposition here for convenience. We also provide an illustrative example of anonymous walks in Fig. 6 to facilitate understanding.

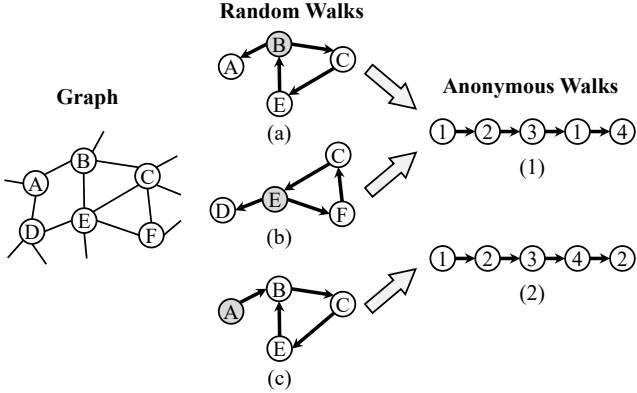


Figure 6: Anonymous walks examples with the starting node colored in grey. Random walks (a) and (b) share the same anonymous walk type, even though the node sets are different. The same node collections may refer to different anonymous walk types as walk (a) and (c).

**Definition 5 (Anonymous Walk).** *Given a random walk  $w = (v_0, v_1, \dots, v_L)$  on a graph, the corresponding anonymous walk is defined as a sequence of integers  $a = (\gamma_0, \gamma_1, \dots, \gamma_L)$ , where  $\gamma_i = \min \text{pos}(w, v_i)$ , and  $\text{pos}(w, v_i)$  returns the position at which the node  $v_i$  first appears in the walk  $w$ . We denote the mapping of a random walk  $w$  to the anonymous walk  $a$  by  $w \mapsto a$ .*

**Proposition 3.** *Let  $G = (\mathcal{V}, \mathcal{E})$  be a graph and  $v \in \mathcal{V}$ . A sufficiently rich distribution  $\mathcal{D}_l$  over length- $l$  anonymous walks starting at  $v$  with  $l = \mathcal{O}(|\mathcal{E}'|)$ , is sufficient to reconstruct the ego graph  $\mathcal{B}(v, h) = (\mathcal{V}', \mathcal{E}')$  centered at  $v$  with radius  $h$ .*

*Proof.* Refer to the proof of Theorem 1 in (Micali and Zhu 2016).  $\square$

### Proof of Proposition 2

**Proposition 4.** *Let  $\mathcal{H} = \{H_i\}_{i=1}^N$  be a sufficiently set of hidden graphs, and let  $\mathcal{K}^{(p)}$  be a positive-definite random walk kernel that distinguishes all non-isomorphic subgraphs of bounded size. If  $\rho$  is injective, then the representation  $c_v^{(t+1)}$  computed by MoSE is injective over the set of  $G_v$ , i.e., MoSE simulates one round of SWL node refinement.*

*Proof.* Since  $\mathcal{K}^{(p)}$  is positive-definite and  $\mathcal{H}$  is sufficiently rich, for any pair of non-isomorphic subgraphs  $G_v \not\cong G_u$ , there exists at least one hidden graph  $H_j \in \mathcal{H}$  such that  $\mathcal{K}^{(p)}(G_v, H_j) \neq \mathcal{K}^{(p)}(G_u, H_j)$ . Hence,  $\Phi(G_v) \neq \Phi(G_u)$ . As  $\rho$  is injective, this implies  $c_v^{(t+1)} \neq c_u^{(t+1)}$ . Therefore, the overall mapping  $G_v \mapsto c_v^{(t+1)}$  is injective over the set of rooted subgraphs, consistent with the SWL refinement definition.  $\square$

### Proof of Corollary 1

**Corollary 2.** *Let  $G$  and  $G'$  be two graphs, and let  $\pi$  denote a fixed subgraph extraction policy. If the SWL test distinguishes  $G$  and  $G'$  under policy  $\pi$ , then MoSE also distinguishes  $G$  and  $G'$  under the same policy, provided the conditions in Prop. 4 hold.*

We prove the corollary by introducing the following definition (Zhang et al. 2023; Feng et al. 2023) and lemma first.

**Definition 6.** *Let  $C_1$  and  $C_2$  be two color refinement algorithms, and denote  $c_i(G)$ ,  $i \in \{1, 2\}$  as the graph representation computed by  $C_i$  for graph  $G$ . We say:*

- $C_1$  is no less powerful than  $C_2$ , if there exist a pair of non-isomorphic graphs  $G$  and  $G'$  such that  $c_1(G) \neq c_1(G')$  and  $c_2(G) = c_2(G')$ .
- $C_1$  is more powerful than  $C_2$ , if for any pair of graphs  $G$  and  $G'$ , if  $c_2(G) \neq c_2(G')$ , then  $c_1(G) \neq c_1(G')$ .

**Lemma 1.** *If the color of nodes in a graph cannot be further refined by  $C_2$  when initialized with the stable coloring from  $C_1$ , then  $C_1$  is more powerful than  $C_2$ .*

The above lemma allows us to assess the relative expressive power of two color refinement algorithms on a single graph instead of requiring a pair of graphs for comparison. We now prove that MoSE is more powerful than SWL.

*Proof.* Given a graph  $G$ , let  $c_v^M$  denote the stable color of node  $v$  from MoSE. We take these stable colors as the initial colors of SWL, i.e.,  $c_v^{S,(0)} = c_v^M$ . For the first SWL iteration, we have:

$$c_v^{S,(1)} = \text{hash}(G_v^{S,(0)}) = \text{hash}((\mathcal{V}_v, \mathcal{E}_v, c_v^M)) \quad (17)$$

Now consider two arbitrary nodes  $v, u$ .

- (i)  $c_v^M = c_u^M$ . By Prop. 4, the rooted subgraphs  $G_v$  and  $G_u$  are color-isomorphic under  $c^M$ , hence the injectivity of the hash yields  $\text{hash}(G_v^{S,(0)}) = \text{hash}(G_u^{S,(0)})$  and therefore  $c_v^{S,(1)} = c_u^{S,(1)}$ . Thus, SWL cannot split a color class that MoSE has already formed.
- (ii)  $c_v^M \neq c_u^M$ . Again by Prop. 4 the subgraphs  $G_v$  and  $G_u$  are not color-isomorphic, so  $\text{hash}(G_v^{(0)}) \neq \text{hash}(G_u^{(0)})$  and consequently  $c_v^{S,(1)} \neq c_u^{S,(1)}$ . Hence, SWL never merges two distinct MoSE classes.  $\square$

## Experimental Supplementary

### Training Procedure of MoSE

#### Algorithm 1: Training Procedure

---

**Input** : Extracted Subgraphs  $G_v = (\mathcal{V}_v, \mathcal{E}_v)$  for  $v \in \mathcal{V}$ ; Subgraph Experts  $E = \{E_s : s = 1, \dots, K\}$  where  $E_s = \{H_1^s, \dots, H_N^s\}$  with hidden graphs

**Output:** Node Embeddings  $\mathbf{h}(v)$  for  $v \in \mathcal{V}$ , Learned hidden graphs

```

1 for epoch = 1, ..., M do
2   for  $v \in \mathcal{V}$  do
3     Calculate the expert scores and select experts via Eqs.(7)-(9);
4     Compute MoE loss  $\mathcal{L}_{importance}$  via Eq. (15);
5     for  $p = 1, \dots, P$  do
6       Calculate the  $p$ -step random walk kernel between  $G_v$  and  $H_i$  in selected experts via Eq. (11);
7       Concatenate the kernel values and map the results as  $\mathbf{h}_s(v)$  via Eq. (10);
8       Combine the node embedding with expert scores as  $\mathbf{h}(v)$  via Eq. (12);
9       (Readout the graph embedding  $\mathbf{h}(G)$  for graph-level task);
10      Compute the task loss  $\mathcal{L}_{task}$ ;
11      Final loss  $\mathcal{L} = \mathcal{L}_{task} + \beta \cdot \mathcal{L}_{importance}$ ;
12      Back propagation, update parameters;

```

---

#### Dataset Details and Statistics

We here introduce the details of the datasets used in our work.

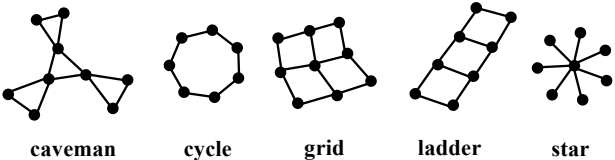


Figure 7: Illustration of the 5 types of graphs in synthetic dataset GraphFive

**Graph Classification Datasets.** We choose 10 datasets, including 8 real-world graphs and 2 synthetic graphs.

For real-world graphs, MUTAG (Debnath et al. 1991), D&D (Dobson and Doig 2003), NCI1 (Wale, Watson, and Karypis 2008), PROTEINS, and ENZYMES (Borgwardt et al. 2005) are bio/chemo-informatics datasets. MUTAG consists of 188 mutagenic aromatic and heteroaromatic nitro compounds. The task is to predict whether or not each chemical compound has mutagenic effects on the Gram-negative bacterium *Salmonella typhimurium*. D&D contains over a thousand protein structures. Each protein is a graph

whose nodes correspond to amino acids. The task is to predict if a protein is an enzyme or not. NCI1 contains more than four thousand chemical compounds screened for activity against non-small cell lung cancer and ovarian cancer cell lines. PROTEINS consists of proteins represented as graphs where vertices are secondary structure elements, and there is an edge between two vertices if they are neighbors in the amino-acid sequence or in 3D space. The task is to classify proteins into enzymes and non-enzymes. ENZYMES contains 600 protein tertiary structures obtained from the BRENDA enzyme database. Each enzyme is a member of one of the Enzyme Commission top level enzyme classes. IMDB-BINARY, IMDB-MULTI, and REDDIT-BINARY (Yanardag and Vishwanathan 2015) are social interaction datasets. IMDB-BINARY and IMDB-MULTI are created from IMDB, an online database of information related to movies and television programs. The graphs contained in the two datasets correspond to movie collaborations. The vertices of each graph represent actors/actresses and two vertices are connected by an edge if the corresponding actors/actresses appear in the same movie. The task is to predict which genre an ego-network belongs to. REDDIT-BINARY contains graphs that model the social interactions between users of Reddit. Each graph represents an online discussion thread. The task is to classify graphs into either communities or subreddits.

For synthetic datasets, we follow (Wang et al. 2024) to generate GraphFive and GraphCycle. For GraphFive, we first generate 8-15 Barabási-Albert graphs as communities, each containing 10-200 nodes. Then, we connect the generated BA graphs in pre-defined five shapes: caveman, cycle grid, ladder, and star. To connect nodes in different clusters, we randomly add edges with a probability ranging from 0.05 to 0.15. We give an illustration of the 5 types of graphs in Fig. 7. For GraphCycle, we first generate 8-15 Barabási-Albert graphs as communities, each containing 10-200 nodes. Then, we connect the generated BA graphs in pre-defined two shapes: Cycle and Non-Cycle. To connect nodes in different clusters, we randomly add edges with a probability ranging from 0.05 to 0.15. The statistics of these datasets are shown in Tab. 4.

**Node Classification Datasets.** We choose 9 datasets, including 3 homophilous graphs and 6 heterophilous graphs. For homophilous graphs, we choose the most common citation networks (Kipf and Welling 2017): Cora, Citeseer, and Pubmed as our homophilic datasets. In these citation networks, nodes represent articles and edges represent the citation relationship between them. Node features are the word vectors and labels are the scientific fields of the papers. For heterophilous graphs, we consider Wikipedia networks (Chameleon and Squirrel), Actor co-occurrence network (Actor), and WebKB (Cornell, Texas, and Wisconsin) (Pei et al. 2020) as small-scale heterophilic datasets. Wikipedia networks consist of web pages and mutual links between them. Node features are the informative nouns on these pages while the labels correspond to the monthly traffic of the page. Actor co-occurrence network is an induced subgraph of the film-director-actor-writer network.

Table 4: Statistics of the graph classification datasets

Dataset	MUTAG	D&D	NCI1	PROTEINS	ENZYMES	IMDB-BINARY	IMDB-MULTI	REDDIT-BINARY	GraphFive	GraphCycle
# Graphs	188	1,178	4,110	1,113	600	1,000	1,500	2,000	5,000	2,000
Type	Biochem	Biochem	Biochem	Biochem	Biochem	Social	Social	Social	Synthetic	Synthetic
Max # Nodes	28	5,748	111	620	126	136	89	3,782	225	513
Min # Nodes	10	30	3	4	2	12	7	6	133	122
Avg # Nodes	17.9	284.3	29.9	39.1	32.6	19.8	13.0	429.6	174.8	299.7
Max # Edges	33	14,267	119	1,049	149	1,249	1,467	4,071	1,480	2,346
Min # Edges	10	63	2	5	1	26	12	4	682	618
Avg. # Edges	19.8	715.7	32.3	72.8	62.1	96.5	65.9	497.8	1033.5	1,641.5
# Class	2	2	2	2	6	2	3	2	5	2

Each node denotes an actor with features representing keywords in Wikipedia. Each edge denotes the collaborations, and node labels are the types of actors. Nodes in WebKB represent web pages and edges are hyperlinks between them. Node features are the bag-of-words vectors and the labels are identities. The statistics of these datasets are shown in Tab. 5

Table 5: Statistics of the node classification datasets

Dataset	# Nodes	# Edges	# Features	# Classes	Homo.
Cora	2,708	10,556	1,433	7	0.825
Citeseer	3,327	9,104	3,703	6	0.717
Pubmed	19,717	88,648	500	3	0.792
Chameleon	2,277	36,051	2,325	5	0.249
Squirrel	5,201	216,933	2,089	5	0.219
Actor	7,600	29,926	932	5	0.206
Cornell	183	295	1,703	5	0.106
Texas	183	309	1,703	5	0.103
Wisconsin	251	499	1,703	5	0.134

## Experimental Setup

For all datasets, we apply the Adam optimizer, and the hyper-parameters that we tune include the learning rate, the dropout rate, the number of subgraph experts, the number and size of hidden graphs in each subgraph expert, the step length of the random walk kernel, and the hidden dimension. For GK-based GNNs, we extract node representations from the layer right before the readout operation and attach a two-layer MLP for the node classification task. The model is implemented with the deep learning library PyTorch 2.2.0 and PyG 2.4.0, running on a Linux server with the Intel(R) Xeon(R) Silver 4210R CPU @ 2.40GHz, the NVIDIA RTX 3090 GPU (24 GB), and 128 GB memory.

## Hyperparameter Sensitivity Analysis

To better understand the robustness and stability of MoSE, we conduct sensitivity analyses with respect to two critical hyperparameters: the number of hidden graphs per expert, and the number of steps used in the Random Walk Kernel (RWK). All experiments in this section are trained for 50 epochs to control training time, and only the hyperparameter on the x-axis is varied, with all other model settings fixed.

As shown in Fig. 8(a), increasing the number of hidden graphs generally improves model performance across most datasets, especially in the early range. This is because

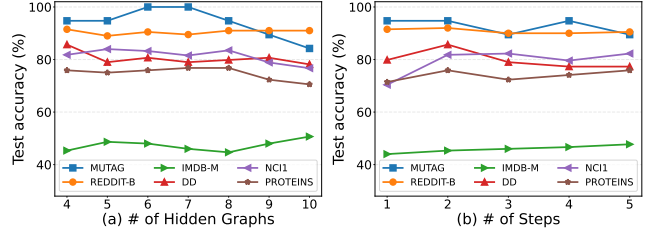


Figure 8: Sensitivity analysis of MoSE with respect to (a) the number of hidden graphs per expert and (b) the number of random walk steps.

more hidden graphs allow the model to better capture diverse structural patterns within each expert. However, we observe diminishing returns or even performance drops beyond a certain threshold, as on PROTEINS and NCI1, likely due to overfitting or increased optimization difficulty. These results highlight the importance of balancing representation capacity and generalization. We also investigate how the number of steps used in random walks affects the model performance in Fig. 8(b). Increasing the number of steps enriches the expressiveness of extracted walk patterns. For most datasets, performance improves up to 3 or 4 steps and then saturates or slightly drops. This suggests that excessively long walks may introduce noise or redundant information, especially for smaller graphs like MUTAG or DD. Thus, a moderate step size provides a good trade-off between expressiveness and efficiency.

## Additional Visualizations

To further demonstrate the behavior of our model, we provide additional visualizations of the learned subgraph experts on four datasets: Chameleon, IMDB-MULTI, MUTAG, and Wisconsin. For Chameleon and IMDB-MULTI in Fig. 9, we visualize the selected subgraph experts as determined by the MoE routing mechanism. These examples highlight how different experts are activated for different subgraph structures, capturing diverse local patterns relevant to node or graph-level tasks.

In contrast, for Wisconsin and MUTAG, we visualize all subgraph experts without filtering by the MoE selection in Fig. 10 and Fig. 11. In these visualizations, each row corresponds to a different expert, and each column represents a hidden graph in that expert. This exhaustive presentation reveals the redundancy among hidden graphs: several experts

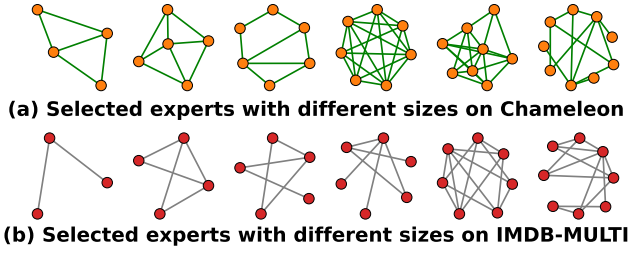


Figure 9: Selected subgraph experts visualization on Chameleon and IMDB-MULTI.

produce similar or uninformative patterns that are eventually filtered out by the gating mechanism. Interestingly, we observe that on simpler datasets such as MUTAG, there is a higher degree of redundancy across experts, indicating that fewer unique subgraph patterns are needed to solve the task. Conversely, Wisconsin, which contains more nuanced structural information, exhibits less redundancy and benefits from a richer set of subgraph experts to capture its underlying characteristics.

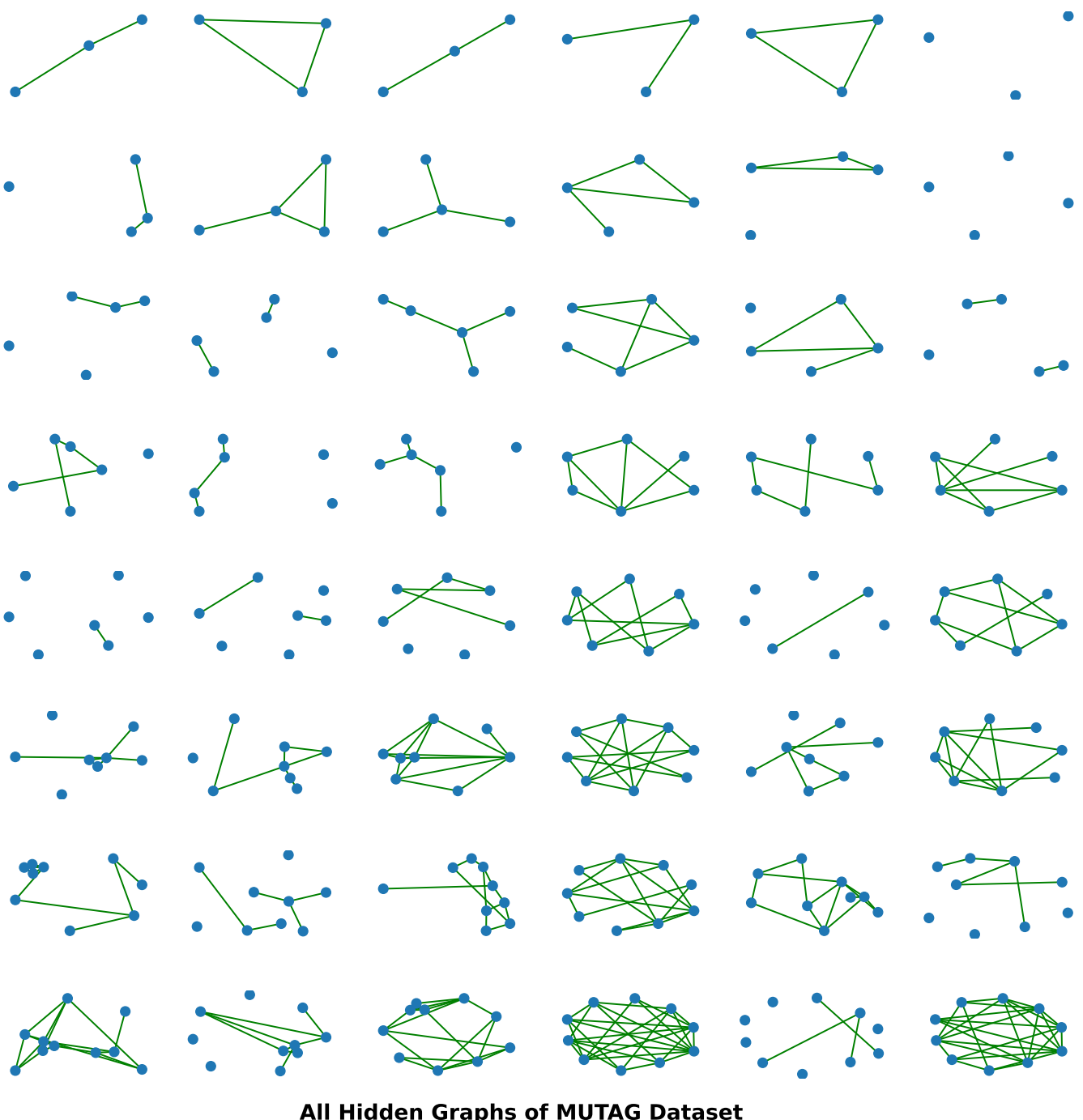
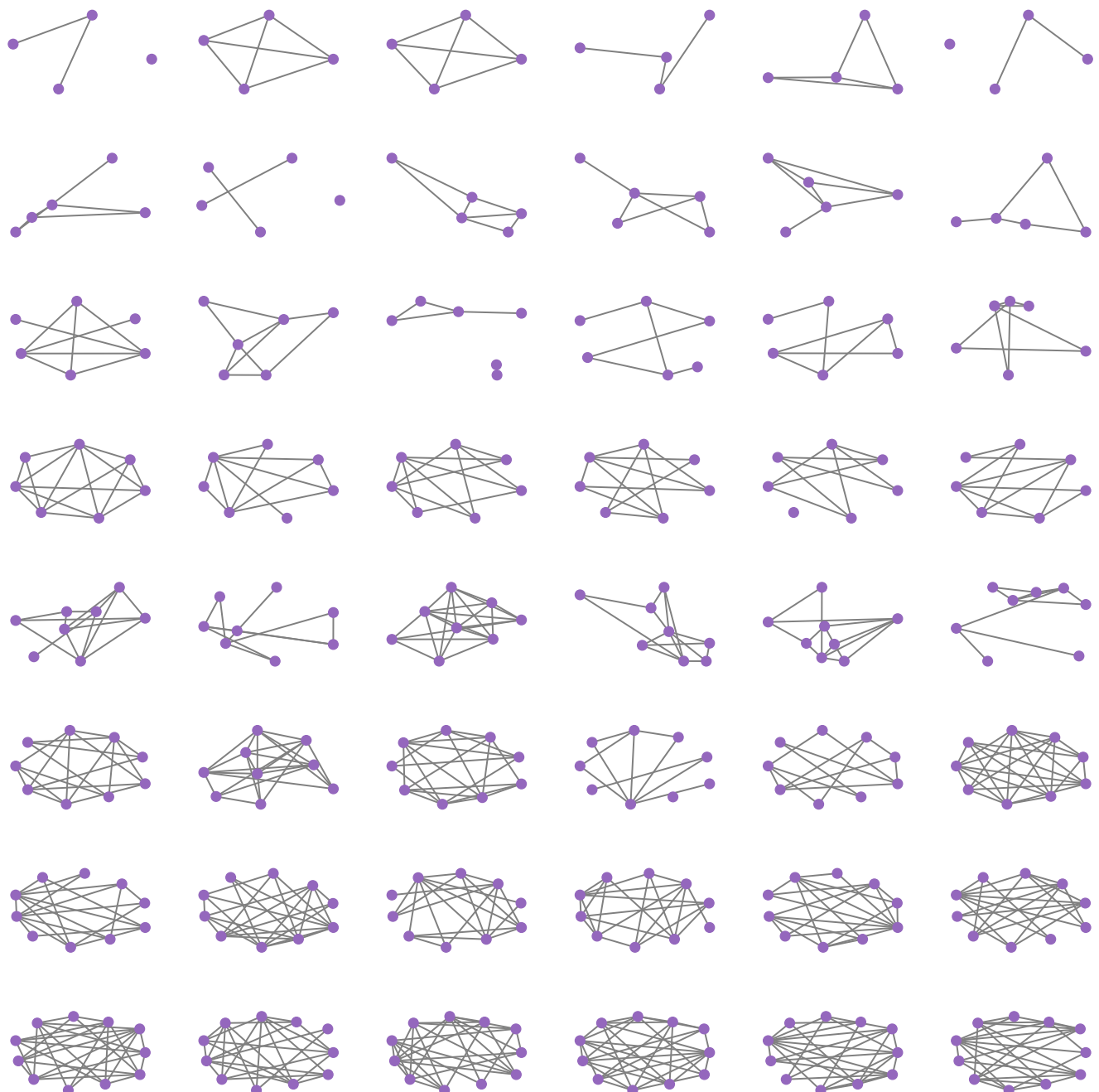


Figure 10: All hidden graphs of MUTAG, regardless of MoE selection. Each row corresponds to a different expert, and each column represents a hidden graph in that expert.



**All Hidden Graphs of Wisconsin Dataset**

Figure 11: All hidden graphs of Wisconsin, regardless of MoE selection. Each row corresponds to a different expert, and each column represents a hidden graph in that expert.